The new High Resolution Ultra Small Angle Neutron Scattering instrument at the High Flux Reactor in Grenoble

Martin Hainbuchner,[a]* Mario Villa,[a] Gerhard Kroupa,[a,b] Gudrun Bruckner,[a,b] Matthias Baron,[a,b] Heinz Amenitsch,[c] Erwin Seidl[a] and Helmut Rauch[a]

[a] *Atominstitut der Österreichischen Universitäten, A-1020 Wien, Austria,* [b] *Institute Laue-Langevin, F-38042 Grenoble, France and* [c]*Institute of Biophysics and X-ray Structure Research, A-8010 Graz, Austria.*
E-mail: hainbuch@ati.ac.at

In 1998, the combined Interferometer and Ultra Small Angle Neutron Scattering (USANS) instrument S18 at the 58 MW High Flux Reactor at the Institute Laue–Langevin in Grenoble (France) started operation. The instrument has been upgraded to allow more advanced neutron optics experiments for fundamental, nuclear and condensed matter physics. The new supermirror guide along with the two channel cut silicon perfect crystals, configured as an advanced high resolution Bonse-Hart camera, provides optimal intensity conditions. A large range of wavelengths is accessible by variations of the Bragg angle and by using different reflecting planes of a properly cut silicon monochromator block in combination with different channel-cut analyzer crystals. The fine adjustment analyzer system is achieved by an advanced piezo drive, which has an accuracy of 0.036 seconds of arc.
The basic features of the USANS camera, which takes advantage of a new tail suppression method, and the results of various test measurements concerning intensities, long term stability and the accessible wavelength range will be presented. A high resolution position sensitive detector can either be used to analyze beam profiles or to perform neutron radiography experiments.

1. Introduction

Due to the installation of the new supermirror guides at the 58 MW High Flux Reactor (HFR) at the Institute Laue-Langevin (ILL), the intensity at the monochromator position has been increased by a factor of five up to 3.9×10^9 n cm^{-2} s^{-1} and the signal to background conditions have been improved considerably. The neutron interferometer set-up S18 has been upgraded to a triple axes instrument and an advanced Bonse-Hart ultra small angle scattering camera has been added (Kroupa et al., 1999). Both instruments use a highly vibration isolated optical bench and a common data acquisition system. Here we focus on recent experiments performed with the Bonse-Hart camera (Bonse & Hart, 1965), which has been adapted to a recently developed tail suppression method (Agamalian, Wignall & Triolo, 1997; Agamalian et al., 1998). This option has also been used for neutron tomography experiments (Biermann, 1998). A diagram of the ultra small angle scattering setup is shown in figure 1. After two years of re-designing and re-building the instrument, in April 1998 the new set-up started operation. Several test measurements have been done in the field of ultra small angle neutron scattering and neutron interferometry.

2. The instrument

The essential parts of the combined USANS and interferometer instrument are placed upon an optical bench, which is isolated against
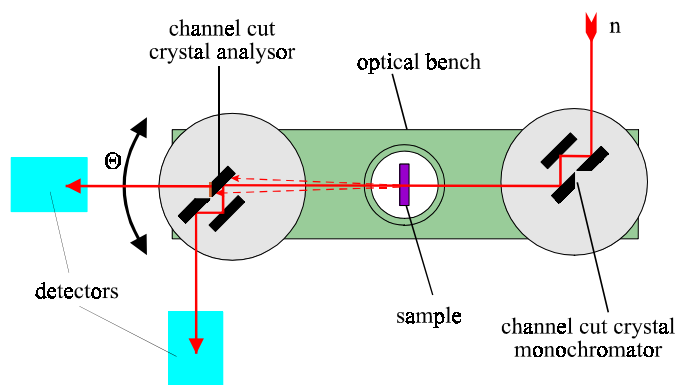

Figure 1
Schematic view of the Bonse-Hart camera at the S18 instrument.

vibrations by a system of springs and oil dampers. The remaining acceleration from vibrations is less than 10^{-6} m/s². The temperature in the instrumental area is controlled by an infra-red heating system.
The temperature achieved is 28°C with a stability of +/-0.1°C. These vibration isolation and temperature stabilizing systems are a necessity for interferometer experiments, while the USANS measurements also are stabilized. The monochromator is placed directly behind the supermirror guide H25, which provides a large divergence of the beam and therefore provides considerably higher intensities compared to the previous set-up. Due to the possibility to rotate the whole instrument from 30° to 150° around the monochromator axis, a wide range of wavelengths is accessible by variations of the Bragg angle and by using different reflecting planes of a properly designed silicon monochromator block. For high resolution USANS applications advanced channel cut crystals, which take advantage of the new tail suppression method, can be used as both monochromator and analyzer crystals. The fine adjustment system of the analyzer axis is achieved by an advanced piezo drive with an angular adjustment range of +/-3.2 degrees and is controlled by an incremental encoder with an accuracy of 0.036 seconds of arc.
Samples and sample environment equipment, like cryostats, magnetic coils, etc. can be introduced between the channel-cut crystals and be adjusted through supports from a separate sample platform mounted above the optical bench. Characteristic parameters of the instrument are summarized in table 1.
The instrument electronics, including the motor controllers for up to 50 stepper motors, the camac readout system, the piezo drive and the vibration damping system are controlled by five networking personal computers. Most of the stepper motors have been equipped with high resolution absolute angle and position encoders.
A high resolution position sensitive detector with a resolution of ~100 µm (Dietze, Felber, Raum & Rausch, 1996) can be used to analyze beam profiles, for radiographic experiments or, together with the Bonse-Hart camera, to perform diffraction enhanced imaging experiments.

3. Test measurements

Various test measurements concerning intensity, resolution, stability and flexibility of the USANS set-up have been performed. Figure 2 shows a typical ultra small angle scattering pattern from a silicon wafer having periodic holes with depth of 100 micrometers and a repeating distance d of 3.5 micrometers. Up to twelve interference orders have been observed in reasonable measuring time. The measured scattering angle between the interference peaks shows excellent agreement with $\Delta\Theta = \lambda / d$.

Table 1

Typical parameters of the new S18 interferometer and USANS set-up.

1. Monochromator axis

Two crystals mounted on a computer controlled support

Type	silicon bloc perfect crystal
Reflecting planes	[111],[220],[113],[115],[117],[331],[335],[551],[400]
Wavelength range	0.6 Å < λ < 5 Å
Bragg angle range	20° < ϑ_B < 55°

Type	silicon channel-cut perfect crystal:
Reflecting planes	triple-bounce [220] Bragg reflection with tail suppression
Wavelength range	1.6 Å< λ < 2.9 Å
Bragg angle range	25° < ϑ_B < 50°

Beam area	~ 2 x 4 cm^2

2. Analyzer axis in Bonse-Hart camera configuration

Second silicon channel-cut perfect crystal

Type	silicon channel-cut perfect crystal
Reflecting plane	triple-bounce [220] Bragg reflection with tail suppression
Peak intensity	10 000 n cm^{-2} s^{-1}
Angular resolution	0.01" (0.04" with absolute encoder)
Momentum resolution	1.5·10^{-5} Å^{-1}
Signal to background ratio	10^5

3. Analyzer axes in single reflection double crystal diffractometer configuration

Second silicon channel-cut perfect crystal

type	[111], [220], [331] single Bragg reflection
Peak intensity	Depends on used reflection (e.g. [220] ~ 16 000 n cm^{-2} s^{-1})
Angular resolution	0.01" (0.04" with absolute encoder)
Beam area	~ 4 x 4 cm^2

4. Analyzer axes in Interferometer configuration

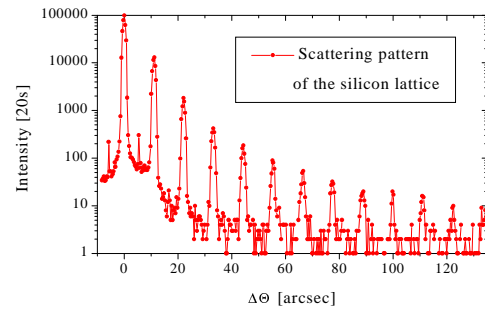*Large perfect Si crystal interferometers of different designs (symmetric, skew symmetric)*

Coherent beam-separation	2 - 5 cm
Enclosed area	up to 25 cm^2
path lengths	14 – 21 cm

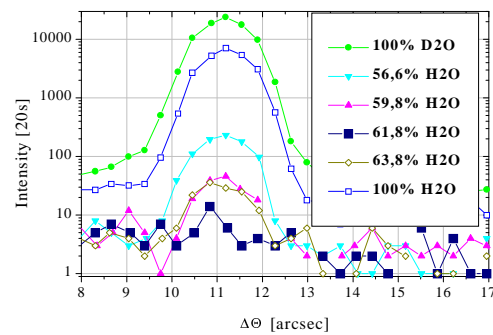*Performance of a [220] skew symmetric interferometer at 1.84 Å with beam area 1x1 cm^2*

flux in front of interferometer	16000 n cm^{-2} s^{-1}
flux in O+H beams	6000 n cm^{-2} s^{-1}
contrast in O beam	> 73 %
Wavelength spread	Δλ/λ = 2.4 % (FWHM)
beam divergence	0.75°

Figure 2

Scattering pattern of a periodic silicon lattice showing twelve interference peaks.

Figure 3

First order peak intensities of a Si structure embedded into a H$_2$O-D$_2$O mixture.

Table 2

Results of solution scattering on Liposome samples

Sample	size[nm]	R$_g$[nm]	R[nm]	I(0)
VitA Acetat	180(70)	157(17)	202	1,62(15)
Tocopheryl Acetat	150(40)	128(11)	165	2,61(16)

The contrast of the interference peaks depends on the scattering length density difference between the Si-matrix and the material inside the holes. This difference can be varied by different D$_2$O-H$_2$O mixtures into which the silicon structure has been put. Figure 3 shows the observed intensity variation of the first order peak.

To demonstrate the resolution limits of the new instrument regarding the low end, e.g. the smallest observable sizes of structures and the small scattering probability, measurements have been performed on Liposomes containing either Probiol Tocopheryl Acetate and Probiol Vitamin A Acetate. Both samples have been provided by KUHS GmbH & Co. Laboratorien, Lörrach-Hanningen. Figure 4 shows the

results of both measurements, in which, as remarkable, the low forward scattering probability of P$_{sc}$(0)=10^{-6} is to be mentioned. The forward scattering probability is defined by (Amenitsch, Rauch & Seidl, 1999):

$$P_{sc}(0) = I_{sc}(0) \, \Delta Q_{min} / (\, \hat{I}_t + \hat{I}_{sc}),$$

where $\hat{I}_{sc}$ and $\hat{I}_t$ are the integrated intensities of the scattered and transmitted neutrons, respectively.

The dimensions of the Liposomes were estimated by the Guinier-approximation, e.g. Guinier (1939). As given in Table 2, the results concerning the particle size show reasonable agreement with the size given by the supplier and which has been determined by Laser Light Scattering.
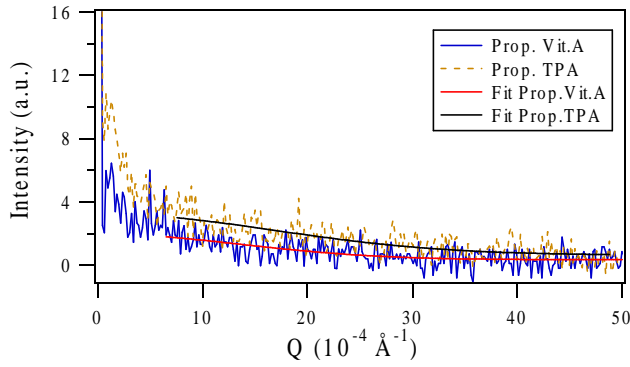
Figure 4
USANS measurements with Liposomes: $P_{SC}(0) \sim 10^{-6}$.

In order to show the flexibility of the S18 set-up, Diffraction Enhanced Imaging (DEI) has been tested (Podurets, Somenkov & Shil´shtein, 1989). As a test sample a glass cylinder with a diameter of 5 mm has been used as an object. Figure 5 shows the standard transmission image with a maximum contrast of 20%. This contrast can be increased by using the diffraction enhanced imaging technique. For that purpose the analyzer crystal of the Bonse-Hart camera has been inserted between the sample and the position sensitive detector. The analyzer crystal has been positioned in the peak of the rocking curve for the central peak image. For the left and right wing images the analyzer crystal has been turned to the left and right slope of the rocking curve at the full width at half maximum position, e.g. Chapman et al. (1997). The results of the diffraction enhanced imaging technique are presented in figure 6. As can be seen, the contrast of the images increases to more than 90% in the left and right wing images. This means, that structures, which are hardly seen in ordinary transmission images, can be made clearly visible by using this technique.

4. Summary

The combined USANS and interferometer set-up S18 is now ready for operation and it shows considerable improvements compared to the previous instrument. The intensity is increased by a factor of five and the signal to background ratio of 10^5 is improved.

The flexibility of the new instrument has been demonstrated by the presented measurements. The solution scattering experiments with low forward scattering probability show that time resolved measurements could also be carried out. Studies on periodic condensed matter structures showed the expected interference peaks for twelve orders, and even more could be achieved. The imaging techniques in combination with the USANS setup also produced satisfying results and will be developed further. Future diffraction enhanced imaging studies, utilizing magnetic field gradients or, in combination with tomographic techniques, will image internal domain structures of ferromagnets.

The combined USANS and interferometer instrument S18 is operated as a CRG-C instrument, which means that it is owned by the Atominstitut in Vienna and access for external users has to be arranged through this channel.
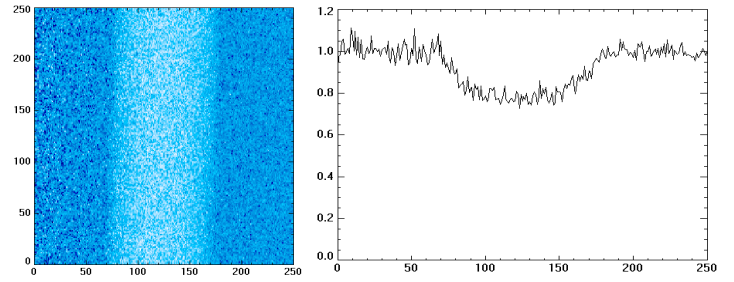

Figure 5
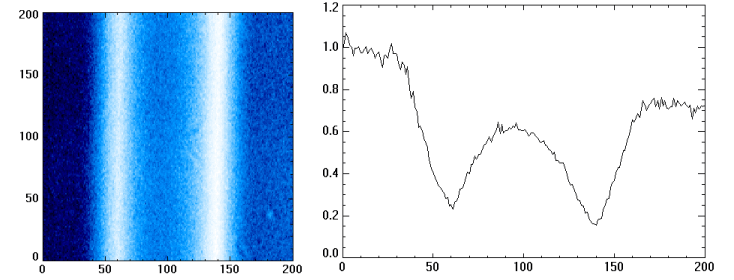Transmission image of a glass cylinder: maximum contrast~20%

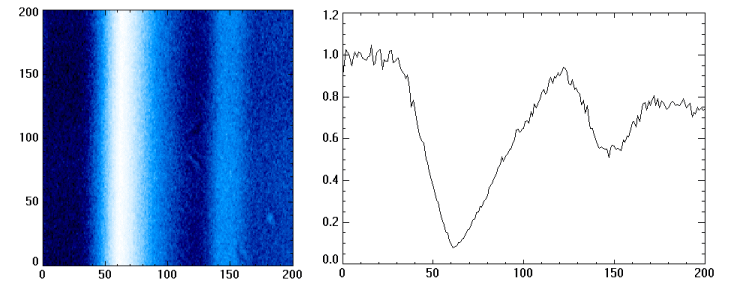**Figure 6a**
DEI at peak position with contrast ~80%

Figure 6b
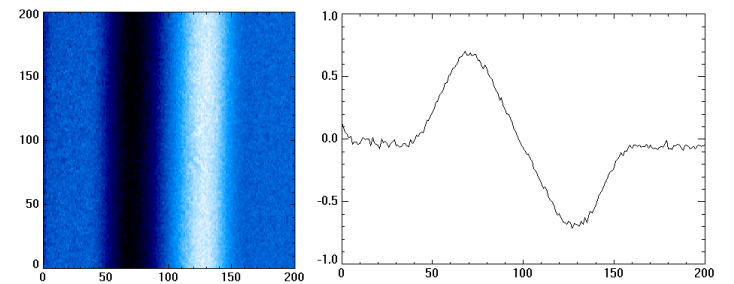DEI at right wing with contrast ~90%

Figure 6c
Calculated DEI Refraction image: $I_R = I_{LW} - I_{RW}$

5. Acknowledgements

6. References

Agamalian, M., Wignall, D. G. & Triolo, R. (1997). *J. Appl. Cryst.* **30**, 345-352

Agamalian, M., Christen, D. K., Drews, A. R., Glinka, C. J., Matsuoka, H. & Wignall, G.D. (1998). *J. Appl. Cryst.* **31**, 235-340

Amenitsch, H., Rauch, H. & Seidl, E. (1999). *Kerntechnik* **64**, in preparation

Biermann, T., in preparation.

Bonse, U. & Hart; M. (1965). *Appl. Phys. Lett.* **7**, 238-240

Chapman, D., Thomlinson, W., Johnston, R.E., Washburn, D., Pisano, E., Gmür, N., Zhong, Z., Menk, R., Arfelli, F. & Sayers, D. (1997) *Phys. Med. Biol.* **42**, 2015-2025

Dietze, M., Felber, J., Raum, K., Rausch, C. (1996) *Nucl. Instr. and Meth. in Phys. Res.* **A377**, 320-324

Guinier, A. (1939). *Ann. Phys.* **12**, 161-167

Kroupa, G. et al., in preparation.

Podurets, K.M., Somenkov, V.A., Shil´shtein, S.Sh., (1989). *Sov. Phys. Tech. Phys.* **34**, 654-65